Projection of Rainfall Intensity-Duration-Frequency Curves at Ungauged Location under Climate Change Scenarios

Muhammad Noor[1], Tarmizi Ismail[2*], Shamsuddin Shahid[2], Md. Asaduzzaman[3], Ashraf Dewan[4]

[1] Department of Civil Engineering, National University of Science & Technology (NUST) Quetta, Pakistan. Email: mnkakar@gmail.com

[2] School of Civil Engineering, Faculty of Engineering, Universiti Teknologi Malaysia (UTM), Johor Bahru 81310, Malaysia. Email: tarmiziismail@utm.my; sshahid@utm.my

[3] Department of Engineering & Design, Staffordshire University, Stoke-on-Trent ST4 2DE, UK. Email: md.asaduzzaman@staffs.ac.uk

[4] Spatial Sciences Discipline, School of Earth and Planetary Sciences, Curtin University, Perth, WA 6102, Australia. Email: a.dewan@curtin.edu.au

* Correspondence: tarmiziismail@utm.my

Projection of Rainfall Intensity-Duration-Frequency Curves at Ungauged Location under Climate Change Scenarios

Abstract

It is vital to quantify the changes in the IDF relationship due to climate change for designing climate-resilient urban hydraulic structures. Such projections are also important for ungauged locations due to the possible urban expansion or human settlements. This work proposed a method for IDF curve construction with associated uncertainty at ungauged locations under climate change scenarios, considering peninsular Malaysia as a case study. The bias in Global Satellite Mapping of Precipitation Gauge Calibrated (GSMaP_GC) data was estimated by comparing its IDF curve with the observed IDF curve. Daily rainfall simulations of four global climate models (GCMs), most suitable for the study area, were employed to approximate the possible alterations in future rainfall distribution for four radiative concentration pathways (RCPs). The results revealed changes in rainfall intensity by -3.4 – 26.7% during 2010–2039, -0.1 – 34.5% in 2040–2069 and -4.3 – 96.8% during 2070–2099 compared to base period 1971–2000 for different RCPs. Overall, the changes were pronounced for short-duration compared to high-duration rainfall. Also, higher emission scenarios showed a greater change than the lower scenarios. The climate change uncertainty range was wider for high-duration and smaller for short-duration. The uncertainty was also higher in the far future.

Keywords: Rainfall intensity-duration-frequency, satellite precipitation, global climate model, uncertainty, bias correction

1. Introduction

Intensity-duration-frequency (IDF) curves illustrate the interrelation among rainfall intensity, duration and frequency. They are essential in many water resources engineering and management fields, including assessing rainfall regimes, classifying rainfall zones, designing stormwater drainage systems, and operating flood control structures (Langousis and Veneziano, 2007; Noor et al., 2018; Tousi et al., 2021; Oberascher et al., 2022). The IDF curves are generally constructed using in-situ rainfall records considering a stationary climate, i.e. considering rainfall changes over time as insignificant (Koutsoyiannis et al. 1998). However, a large change in climate due to global warming is now being recognised (Iqbal et al., 2021; Salman et al., 2020). Rainfall variability has changed significantly in most parts of the world due to changes in atmospheric moisture under a warmer climate (Shahid 2011; Trenberth 2011). A small deviation in the mean value can lead to a big change in extremes. Therefore, an upsurge in intense rainfall has been noticed in many regions (Hajani et al., 2017; Pour et al., 2020; Pour et al., 2014). It means IDF curves developed in a stationary rainfall regime would not be applicable to design hydraulic structures (Rodríguez et al. 2014; Jalaei et al., 2020; Young et al., 2020).

Several attempts have been made to consider nonstationary in constructing IDF curves and supporting climate-resilient hydraulic infrastructure development (Agilan and Umamahesh 2017; Noor et al., 2018; Cheng and AghaKouchak 2014; Ouarda et al. 2019; Yan et al. 2019; Yilmaz and Perera 2014). In most studies, the existing trends in rainfall were incorporated into the rainfall distribution parameters as covariates. For example, Cheng and AghaKouchak (2014) added the trend in historical annual maximum rainfall intensity (AMRI) in probability distribution function (PDF) parameters of AMRI for constructing nonstationary IDF curves. Agilan and Umamahesh (2017) incorporated nonlinear trends in distribution parameters and reported that bias in estimating IDF curves can be minimised by considering the linear trend. A different approach was adopted by Ouarda et al. (2019), whereby the Southern Oscillation Index (SOI) is used as a covariate to produce nonstationary IDF curves. They reported the incorporation of teleconnections and climate change information in the IDF curves could be more reliable under climate change scenarios. However, a major drawback of the existing nonstationary IDF curves is their dependency on the exiting trends in AMRI or the relationship with climate indices. Future changes in climate due to global warming obviously would not follow historical changes (Alamgir et al. 2020). The existing relationship of rainfall with different large-scale indices like SOI would change as well (Khan et al. 2020). However, the climatic change would depend on policies adopted globally to reduce greenhouse gas emissions

and other socioeconomic pathways. Therefore, the IDF curves need to be developed based on projected climate, i.e. different climate change scenarios, to make them effective for climate-resilient infrastructure development.

Global climate models (GCMs) project the changes in rainfall properties over a century. GCM projections have been used in recent years to review and update the IDF curves for adaptation measures in water management infrastructures (Feitoza Silva et al., 2021; Khazaei, 2021). Several assumptions are made in GCM development due to a lack of knowledge on complete details of various earth and atmospheric processes, which cause a large uncertainty in GCM simulations. This also incurs risks in applying IDF curves developed using GCM projected rainfall. Uncertainties in projected IDF curves are generally incorporated to reduce risk in hydraulic design. It is expected that the uncertainty in the projected IDF should not be large, which is the main basis for designing cost-effective hydraulic structures. The selection of a suitable GCM subset based on their skill in estimating present climatology is generally suggested for trustworthy climate simulations (Iqbal et al. 2020; Samadi et al. 2010).

Projection of IDF curves at ungauged locations is a major challenge in hydraulics. Although several studies have been conducted to project IDF curves using GCM and remote sensing data, there is little attempt so far to project IDF curves at ungauged locations. However, such information is essential for developing a long-term climate-resilience society in any region.

This work proposed constructing IDF curves with associated uncertainty at ungauged locations under climate change scenarios. The curves were generated through bias correction of remote sensing rainfall using recorded hourly rainfall data. The GCM projected rainfall was used to project the IDF curves for four representative concentration pathways (RCPs). The methodology proposed in this study can be employed for projecting IDF curves at ungauged locations for climate change scenarios to mitigate the challenge of data scarcity and climate change in hydraulic engineering.

2. Study area and data

2.1 Peninsular Malaysia

Geographically, peninsular Malaysia (1.20º–6.80º N; 100.10º–104.20º E) with an area of 130,598 km^2, is surrounded by Singapore in the south and Thailand in the north. Figure 1 shows the location of peninsular Malaysia and the rain gauges. The rainfall distribution of the study area is influenced by monsoon winds, orography and intricate land-sea boundaries. The

interaction of sea winds with mountains determines precipitation climatology (Khan et al., 2019). Most of the rainfall in peninsular Malaysia is received during the northeastern and southwest monsoons. In addition, extreme rainfall is often reported particularly in the western regions during transitional periods (Suhaila and Jemain 2009). The annual average precipitation of the area ranges between 2000 and 4000 mm, while the temperature ranges from 21 to 32°C (Nashwan et al., 2018; Pour et al., 2020).

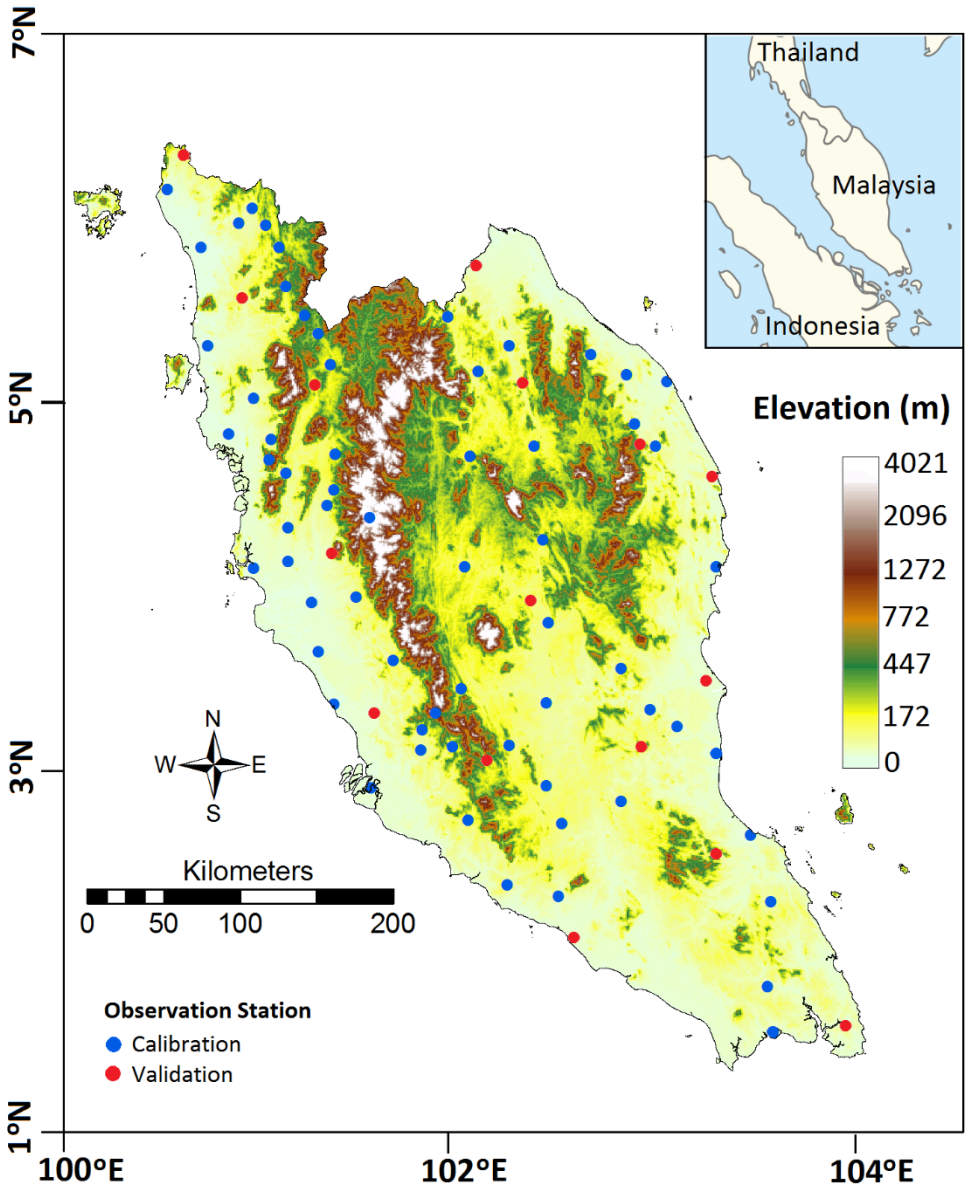

Figure 1 Location of **the** study area and in-situ rain gauges

2.2 Data and sources

The methodology adopted in the current study was implemented in peninsular Malaysia. Observed rainfall data, Global Satellite Mapping of Precipitation gauge calibrated (GSMaP_GC) and Coupled Model Intercomparison Project (CMIP5) GCM's rainfall were used for projecting IDF curves at ungauged locations under climate change scenarios. Table 1 describes the data used in this study.

Table 1 The rainfall datasets utilised in the current study

Rainfall data	Temp resolution	Data period	Spatial resolution	Source
Observed	1-hour	1971-2018	80 stations	DID Malaysia
Global Satellite Mapping of Precipitation V6 gauge calibrated (GSMaP_GC)	1-hour	2000-2018	0.1°×0.1°	https://sharaku.eorc.jaxa.jp/GSMaP/index.htm
Coupled Model Intercomparison Project (CMIP5) Global Climate Models (GCMs)	daily	Historical 1971-2005 Projected 2010-2099		http://www.ipcc-data.org/sim/gcm_monthly/AR5/ Reference-Archive.html

2.2.1 Rainfall data

The in-situ hourly rainfall records of 80 stations for 1971–2018 (Figure 1) were obtained from the Malaysian Department of Irrigation and Drainage (DID). The data homogeneity was evaluated in earlier studies (Noor et al., 2021) which reported adequate quality for hydro-climatic studies. Description of the stations is provided in Supplementary Table S1.

GSMaP_GC rainfall for the period 2000–2018 was utilised for constructing IDF curves at ungauged locations. Previous studies on skill assessment of satellite rainfall datasets revealed that GSMaP_GC is the most suitable for peninsular Malaysia (Noor et al., 2021). Precipitation estimated using passive microwave and infrared radiometers is corrected using the in-situ rainfall data to generate the GSMaP_GC product (Kubota et al., 2007).

2.2.2 GCM Simulations

The GCM simulated daily rainfall data of peninsular Malaysia was collected from the CMIP5 data portal. Noor et al. (2019a) evaluated CMIP5 GCMs in reconstructing historical rainfall climatology and suggested four GCMs most suitable for rainfall projections for peninsular

Malaysia (Table 2). The rainfall projections of these models were used for projecting IDF curves with associated uncertainties.

Table 2 Global Climate Models employed in the current study

Data source	Model	Resolution (lat ×lon)
Beijing Climate Center, China	BCC-CSM1-1(m)	2.8° × 2.8°
National Center for Atmospheric Research, USA	CCSM4	0.94° × 1.25°
Commonwealth Scientific and Industrial Research Organization (CSIRO), Australia	CSIRO-Mk3-6-0	1.8° × 1.8°
Met Office Hadley Centre, UK	HadGEM2-ES	1.25° × 1.875°

3. Methodology

The methodology used for projecting IDF curves at ungauged locations with associated uncertainties is illustrated in Figure 2. The in-situ and GSMaP_GC hourly AMRI series were used to generate corresponding IDF curves and estimate bias in the GSMaP_GC IDF curve. Rainfall data of 80% of stations (64 stations) were used for estimating bias correction parameters, and the remaining 16 stations for evaluating the precision of the developed curves. The bias correction performance was evaluated for different ratios of data divisions, including 60:40, 70:30 and 80:20. A data division ratio of 80:20 was finally used as it provided the best performance. The stations for calibration and validation were selected randomly. The bias correction factor, derived via validation, was then used for correcting bias in the IDF curves at ungauged locations, estimated through GSMaP_CG rainfall (Noor et al., 2021).

The GCM projected daily rainfall for three periods (2010–2039, 2040–2069 and 2070–2099) for four RCPs, i.e. 2.6, 4.5, 6.0 and 8.5, was interpolated at observed grid points. The best-fit PDF for the interpolated daily AMRI, estimated based on the negative likelihood ratio, was used to estimate the changes in the PDF parameters or climate change factor (CCFs) for three future periods compared to the reference period (1971–2000). These CCFs were applied to PDF parameters of AMRI of GSMaP_GC, and the perturbed PDFs were used to project IDF curves.

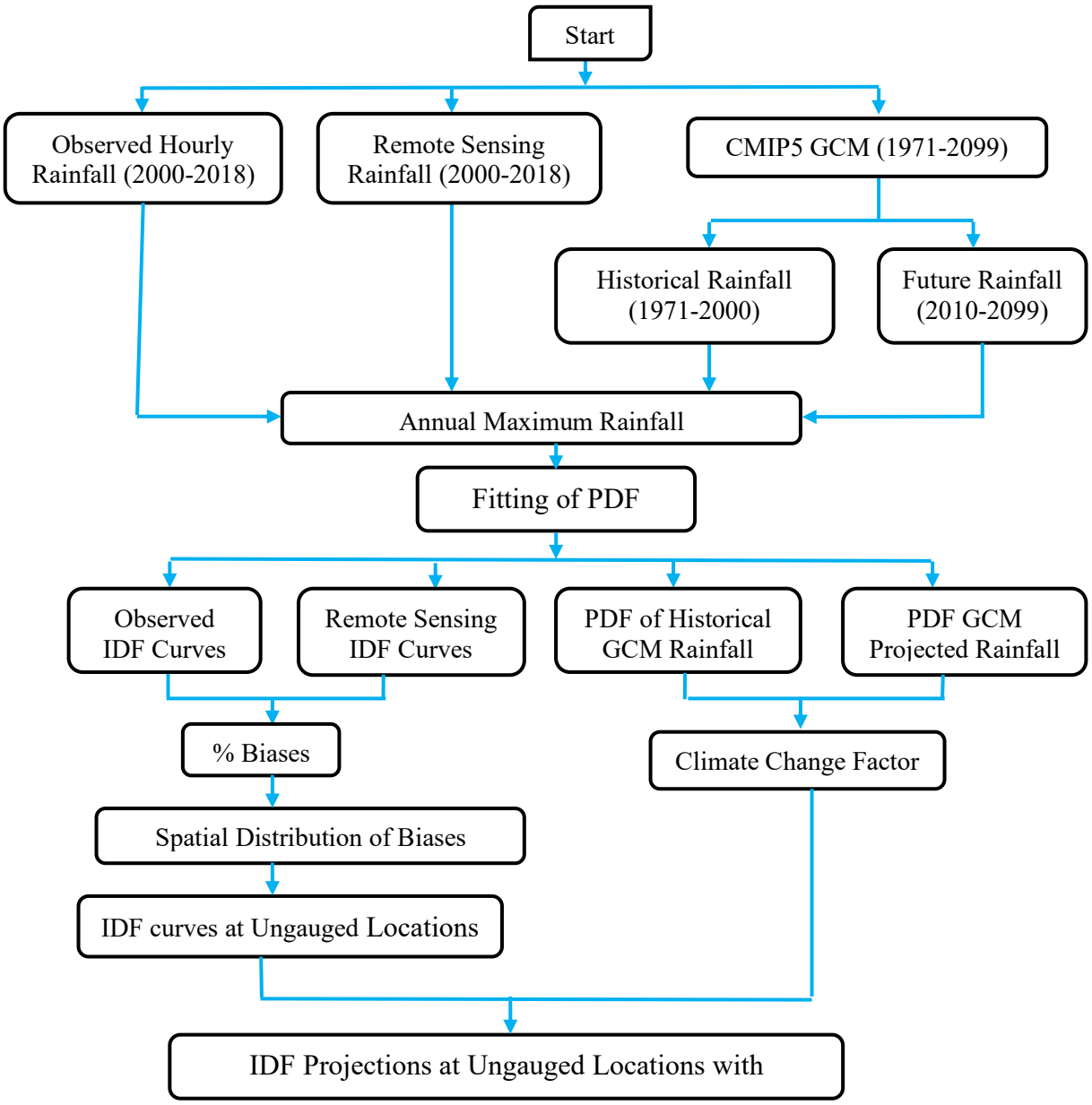

Figure 2 Procedure used for projecting IDF curves with uncertainties at ungauged locations under climate change scenarios

3.1 Bias Correction of Satellite Rainfall IDF Curve

The biases in GSMaP_GC rainfall for 1, 3, 6, 12, 24, 48, 72-hour duration, each for 2, 5, 10, 25, 50, 100 years return periods (RPs) were estimated. The difference in observed IDF and nearest grid point GSMaP_GC IDF was used to estimate bias in GSMaP_GC IDF. Estimated biases at 64 stations were interpolated at all GSMaP_GC grid points using the inverse distance weighting (IDW) function. The IDW was employed as it has been reported to be the most reliable for rainfall interpolation in peninsular Malaysia (Ziarh et al., 2021). Interpolated bias

values were then used to correct biases in GSMaP_GC IDF at 16 validation locations. The interpolated bias in rainfall intensity for all durations and RPs was added to GSMaP_GC rainfall intensity for corresponding durations and RPs to correct the bias of the GSMaP_GC IDF curve. The bias-corrected IDF curves were compared with the observed curves to validate the bias correction method in estimating IDF curves at ungauged locations from GSMaP_GC rainfall. The procedure used for the estimation and correction of bias of GSMaP_GC IDF curves is presented in Figure 3. This procedure has been widely used for correcting bias in IDF curves generated from satellite precipitation (Ombadi et al., 2018; Noor et al., 2021; Venkatesh et al., 2021).

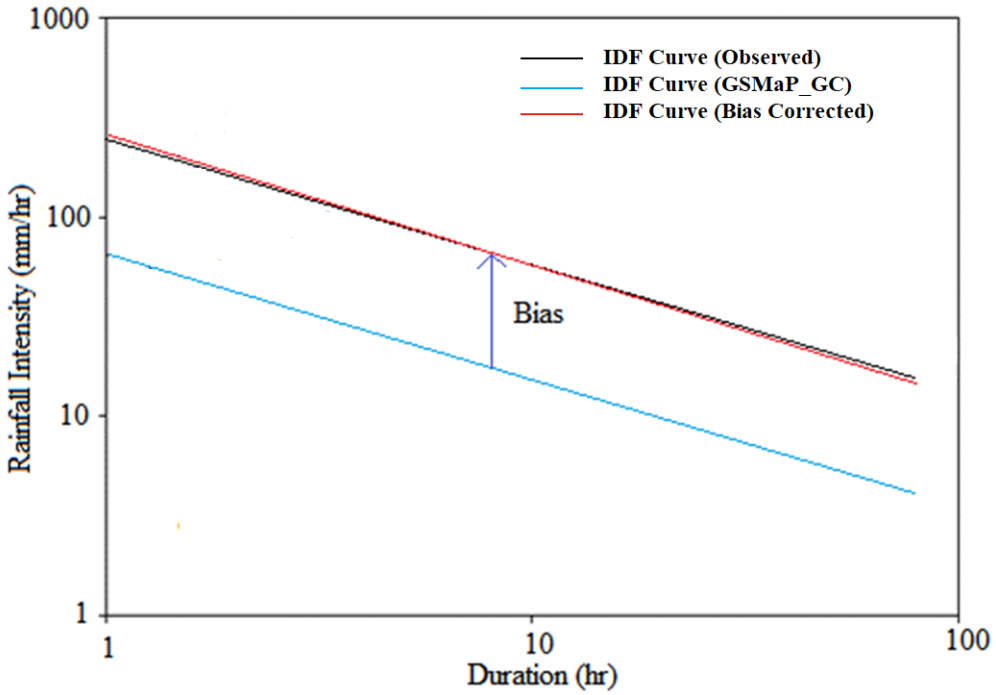

Figure 3 Procedure used for estimation and bias correction of remotely sensed IDF curves

3.2 Projection of IDF Curves at Ungauged Locations

GCM simulated rainfall for the period 1971–2099 was interpolated to the observation station using bilinear interpolation algorithm. This interpolation algorithm is generally used for GCM data interpolation due to its ability to transfer coarse resolution GCMs to fine resolution without changing the GCM simulated climate change signal (Nashwan and Shahid, 2020; Iqbal et al., 2021). The interpolated rainfall at each station for reference (1971-2000) and future periods (2010-2039, 2040-2069 and 2070-2099) was used to estimate daily AMRI for each period. The daily AMRI series for each period was then fitted with a common PDF. The changes in daily

AMRI PDF parameters in the future periods compared with the reference period were estimated as CCF. The CCFs were added with the corresponding PDF parameters of GSMaP_GC AMRI for different durations to approximate AMRI PDFs for future periods. The approximated PDFs were finally used to generate IDFs for different RPs for three future periods and four RCPs. The procedure is elaborated in Figure 4.

Previous studies (Noor et al., 2021; Yusof et al., 2009) showed generalised extreme value (GEV) distribution best fits the daily and hourly rainfall of peninsular Malaysia. The GEV is a three-parameter distribution, scale (σ), location (μ) and shape (k), where σ indicates the spread of the distribution, μ describes the centre of mass (mean) of the distribution and k indicates the influence of the tail structure of distribution. It can be expressed as,

$$F(y) = \exp\left(-\left[1 + k\left(\frac{y}{\sigma} - \mu\right)\right]^{-1/k}\right), \qquad y \geq \sigma(\mu - 1/k). \tag{1}$$

The difference (%) of these three parameters for three future periods for four RCPs compared to the reference period was estimated as shown in Figure 4. GCMs do not provide projections of hourly rainfall. Therefore, it was considered that the shift in GEV distribution of hourly rainfall maxima between the reference period and future period would be the daily rainfall. Similar perturbation of GEV parameters has been previously used for IDF curve projections by Peck et al. (2012) and Ragno et al. (2018).

The CCF for each GEV parameter was estimated as the difference (delta) between GEV parameters fitted to projected (k_p, μ_p, σ_p) and historical (k_h, μ_h, σ_h) daily rainfall, which are presented as Δk, $\Delta\mu$ and $\Delta\sigma$ in Figure 4. The CCFs were added with the GEV distribution parameters of GSMaP_GC hourly rainfall to generate IDF curves for future periods.

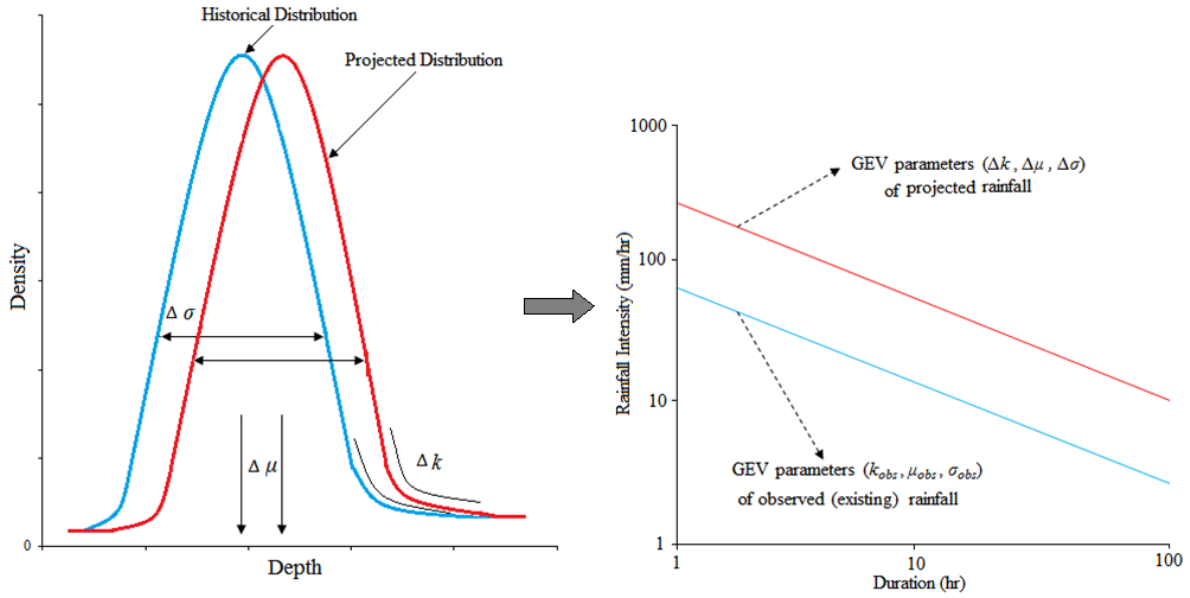

Figure 4 Development of IDF curve for future periods by estimating changes in daily rainfall distribution parameters between the reference and future periods.

The present study estimated the CCF at each GSMaP_GC grid point for three future periods and four RCPs. The IDF curve was generated for each of the four selected GCMs. Their average provided the mean, while the upper and the lower bounds provided the uncertainty range of the IDF curves. The procedure used for projecting IDF curves with uncertainties is presented in Figure 5.

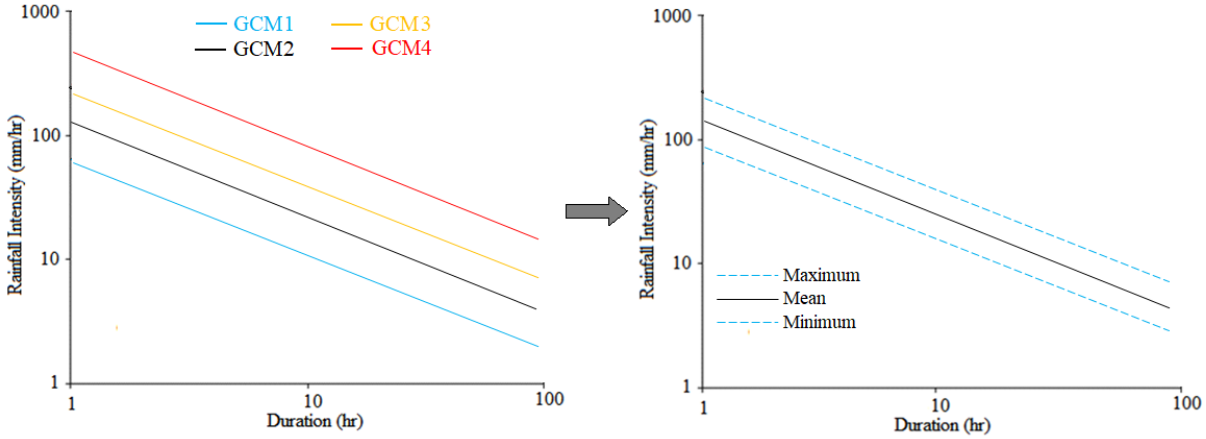

Figure 5 Procedure used for projecting IDF curves with climate change uncertainties

4. Results and Discussion

4. 1 Construction of IDF Curves at Ungauged location

The bias or difference between GSMap_GC IDF curves and the in-situ IDF curves was estimated at 64 stations (80% of available stations). The estimated difference was interpolated at 16 locations, used for validation, and then added with the IDF curves to correct the curves. The estimated difference in rainfall intensity as a percentage of observed rainfall intensity for different RPs of hourly AMRI at 64 stations is presented using boxplots in Figure 6. The results showed less difference for shorter RPs which gradually increases for longer RPs. The long whiskers of the boxes indicate the increase in the spatial variability of bias with RPs.

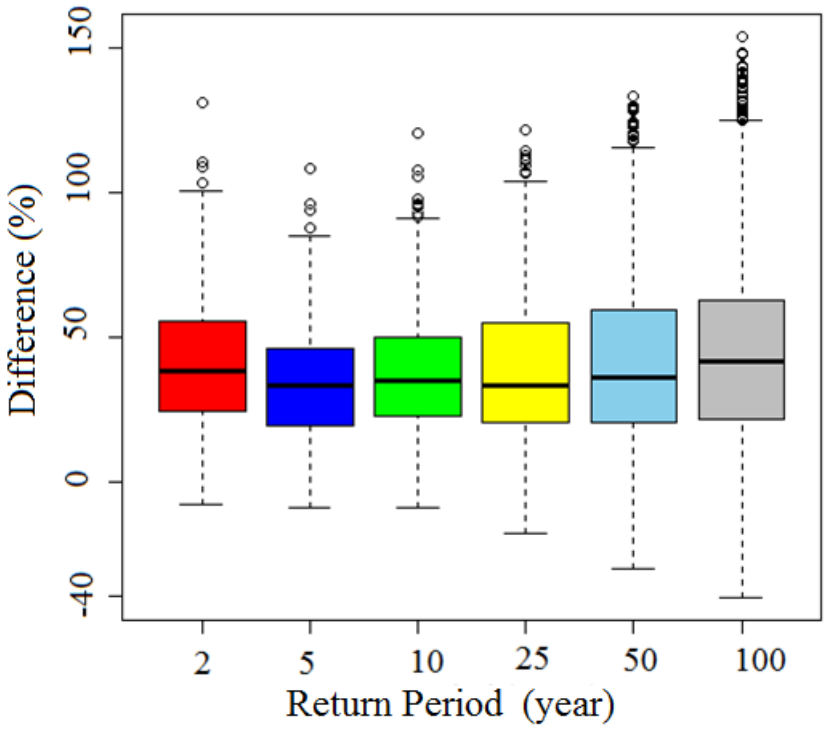

Figure 6 Estimated difference (%) in GSMaP_GC rainfall intensity compared to observed rainfall intensity for different return periods

The corrected IDF curves at 16 validation stations were used to evaluate the reliability of the IDF curves at ungauged locations, estimated using GSMaP_GC rainfall. The obtained results at a station used for validation are shown in Figure 7. The results show a perfect match of IDF curves for all the RPs, constructed using in-situ and bias-corrected GSMaP_GC rainfall. The scatter plot of in-situ and bias-corrected GSMaP_GC rainfall intensity at all 16 stations is shown in Figure 8. The coefficients of determination between in-situ and bias-corrected GSMaP_GC rainfall intensity for all RPs were higher than 0.91. The estimated IDF curves

matched well with the in-situ IDF curves for both the low and high RPs. This indicates the suitability of derived IDF curves at an ungauged location for practical applications. The GSMaP_GC IDF correction result for another station is presented in Supplementary Figure S-1.

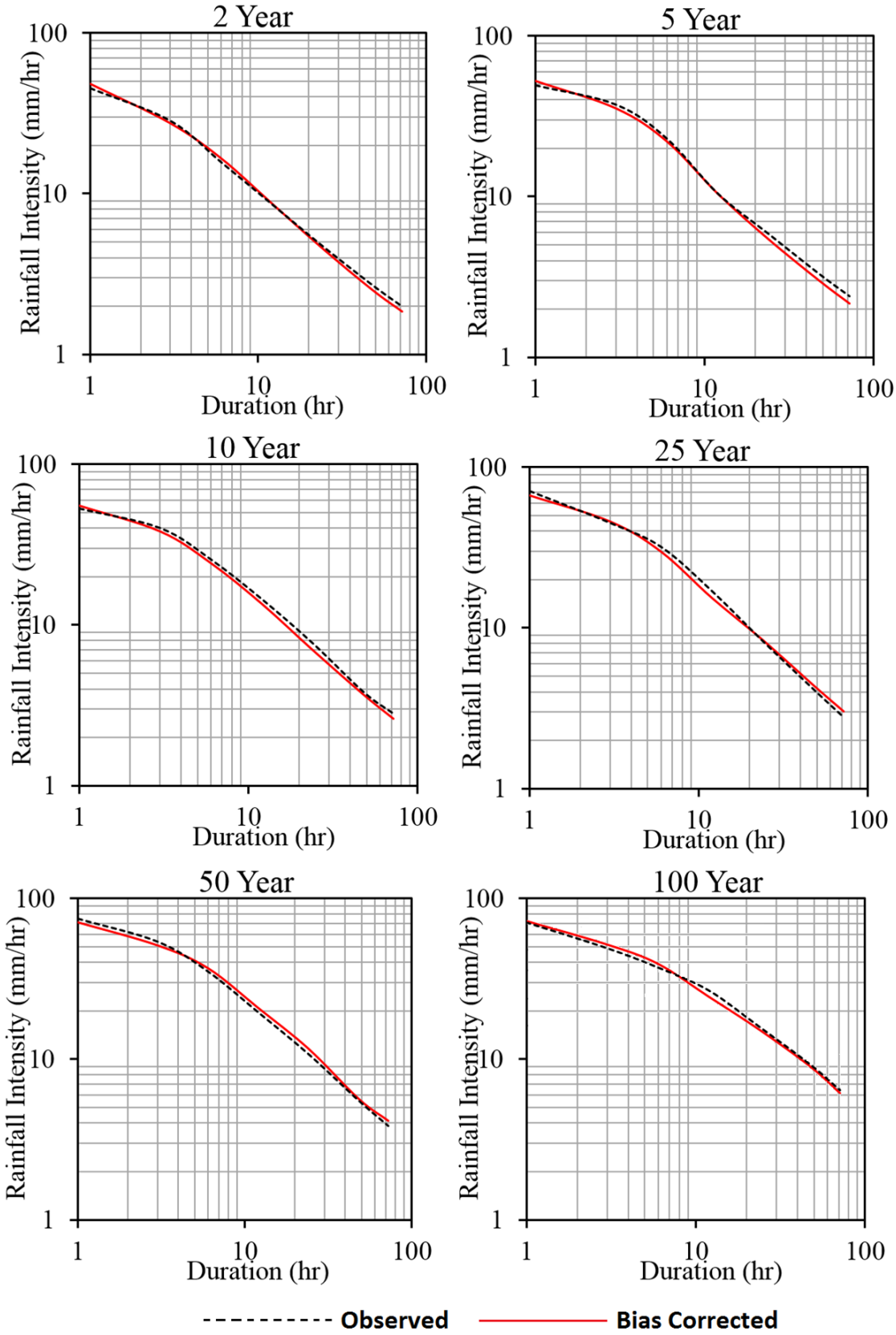

Figure 7 In-situ and corrected GSMaP_GC IDF curves for different return periods at a station located south of peninsular Malaysia, presented as an example.

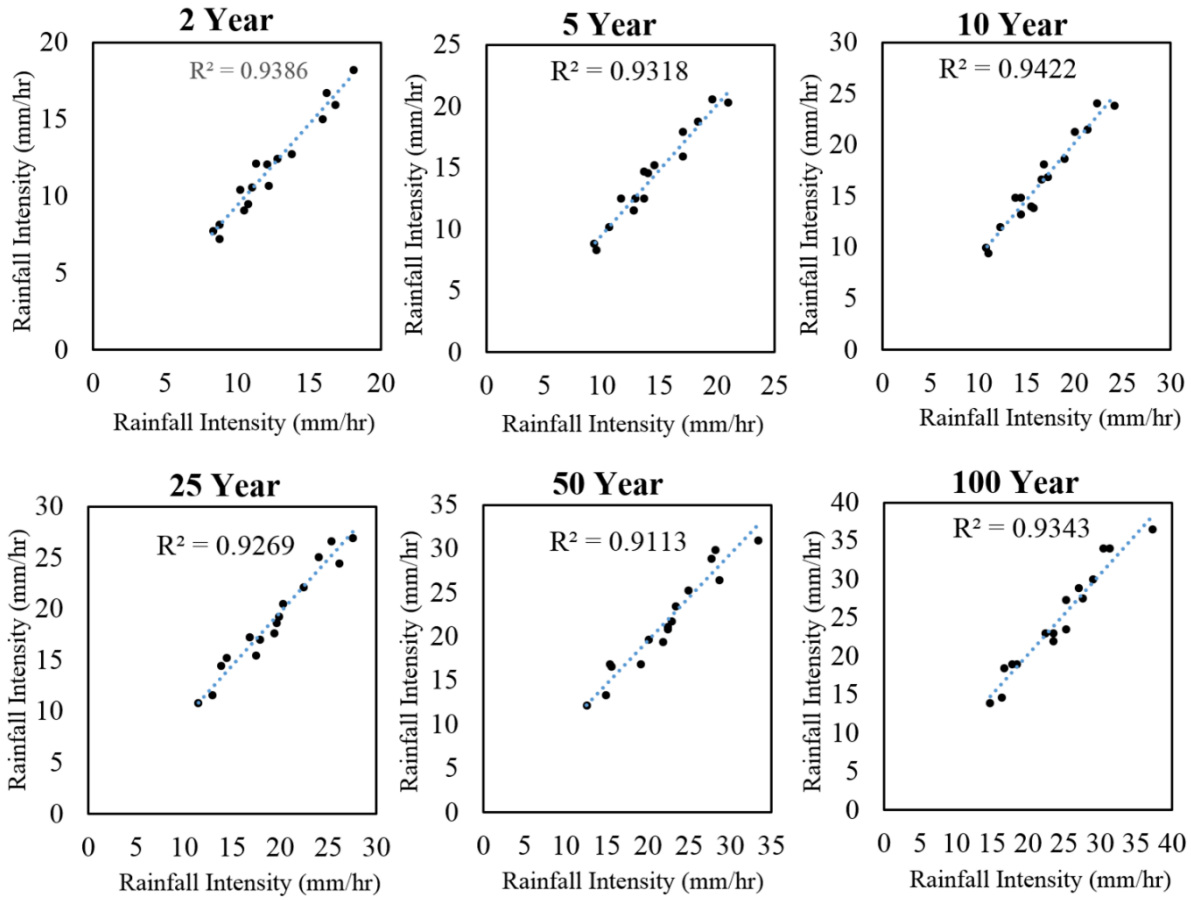

Figure 8 Scatter plot of in-situ and corrected GSMaP_GC rainfall intensity for different return periods at ungagged locations

4.2 Projection of IDF Curve at Ungauged Locations with Uncertainties

The changes in GEV parameters of daily AMRI for future periods in comparison to the reference period at 80 stations were interpolated at all the GSMaP_GC grid points to generate the map of CCFs. The spatial distribution of changes in σ, μ and k of the GEV distribution for BCC-CSM1-1(m) for four RCPs for 2070–2099 in comparison to the reference period (2071–2000) is shown in Figure 9. The change values of GEV parameters interpolated at a GSMaP_GC grid point for a particular scenario and future period were used to perturb the GEV distribution parameters of GSMaP_GC rainfall to generate GEV distribution parameters for that scenario and period. The distribution parameters were then used to construct IDF curves for RCPs. The bias in GSMaP_GC of the location was finally added to project the IDF curve. The IDF curves generated for three future periods and four RCPs for BCC-CSM1-1(m) at a station located south of the peninsula are presented in Figure 10. The lowest changes in IDF were observed for RCP 2.6 and the highest for RCP 8.5. The intensity of rainfall showed an

increase over time, and therefore, the greatest changes in the IDF were projected for 2070-2099.

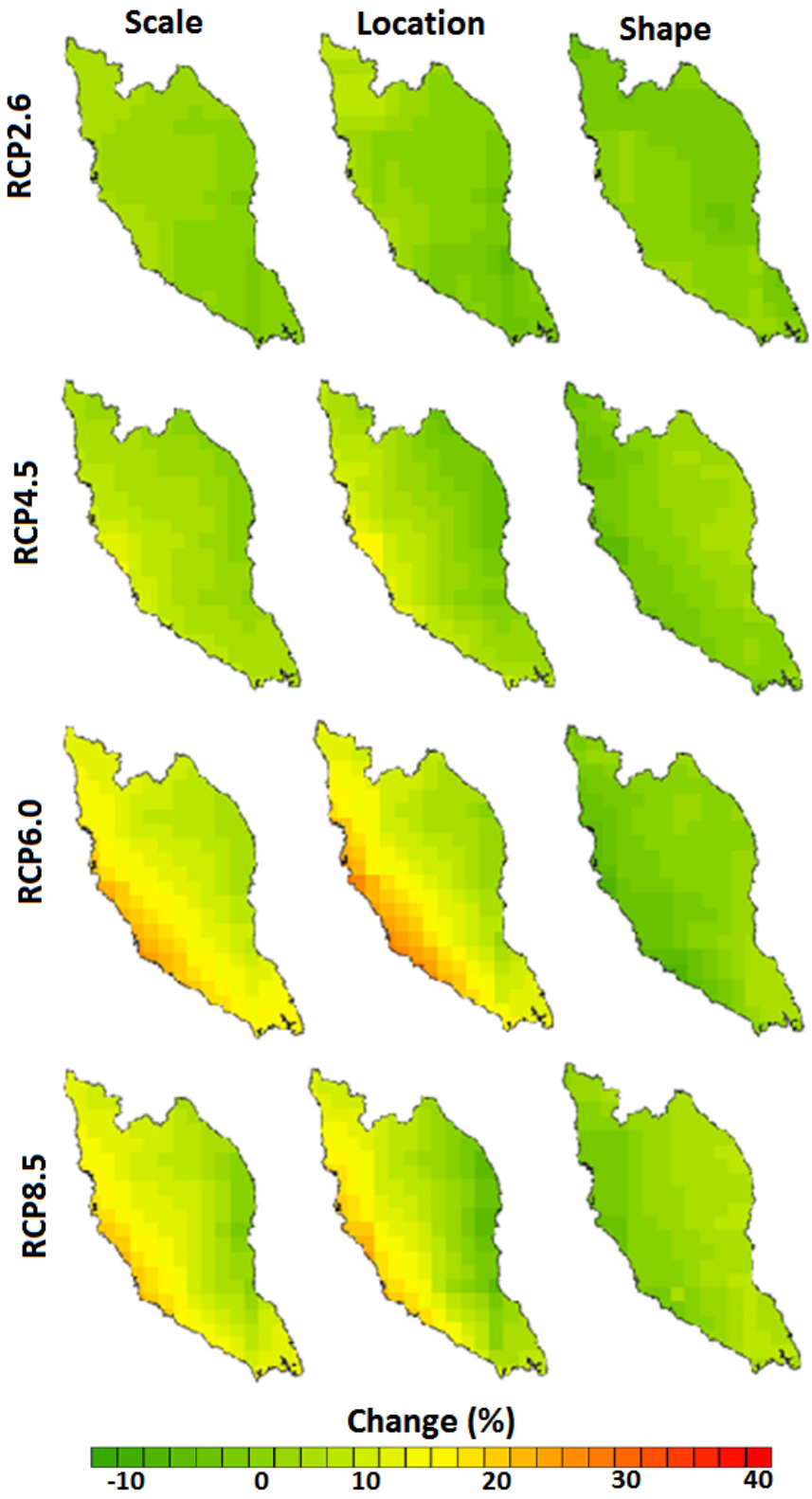

Figure 9 Changes in scale, location and shape parameters during 2070-2099 compared to the reference period (2071–2000) for four RCPs of BCC-CSM1-1(m) at different grid points in peninsular Malaysia

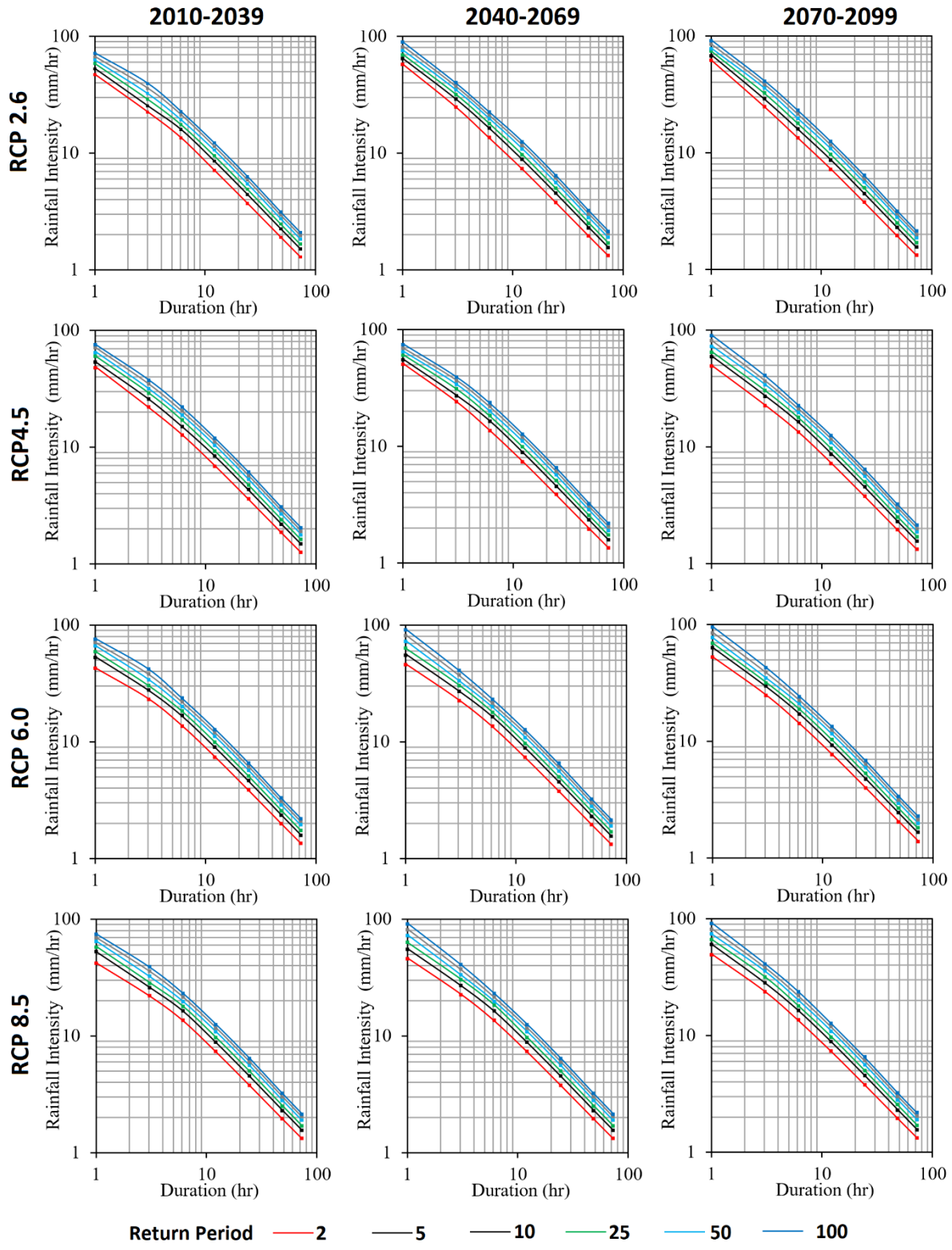

Figure 10 The IDF curves developed for three future periods and four RCP scenarios of BCC-CSM1-1(m) at a station located south of peninsular Malaysia

The projected IDF curves were developed for all the four selected GCMs for four RCPs and three future periods. The mean, upper and lower bounds of the IDF curves of different GCMs were estimated to construct the projected IDF curves with uncertainties. The obtained IDF curves with uncertainty band for (a) RCP 2.6 and (b) RCP 8.5 during 2070-2099 are shown in Figure 11. Overall, uncertainty in the IDF curve was higher for high emission scenarios and far future compared to low emission scenarios and near future. The results also showed a higher increase in short-duration rainfall intensity than large duration rainfall intensity. Particularly, the increase would be more for short duration high RP rainfall intensity. For example, 2-year RP 1-hour rainfall intensity will increase from 53 mm/hr to 65 mm/hr, while 24-hour rainfall intensity will be from 12.1 mm/hr to 15.8 mm/hr for RCP 8.5. In contrast, the 100-year RP rainfall intensity will increase from 70 mm/hr to 95 mm/hr for 1-hour, while from 12.6 mm/hr to 19.6 mm/hr for 24-hour.

The minimum, mean and maximum changes (%) in rainfall return periods in three future periods and four RCPs for whole peninsular Malaysia are presented in Table 3. The results revealed mean changes in the IDF, ranging from 7.5 to 15.5% for 2010–2039, 5.0 to 19.7% for 2040–2069 and 5.0 to 40.7% for 2070–2099 than the base period. The mean changes were in the range of 7.8–8.4% for RCP 2.6, 7.5–8.4% for RCP 4.5, 14.4–15.7% for RCP 6.0 and 12.9–13.5% for RCP 8.5 during 2010–2039. The largest changes were found in the far future (2070–2099) for all scenarios. The projected changes were 5.0–5.5% for RCP 2.6, 10.8–11.8% for RCP 4.5, 24.5–27.9% for RCP 6.0 and 31.0–40.7% for RCP 8.5. The results indicate the projection was high for higher scenarios and the far future.

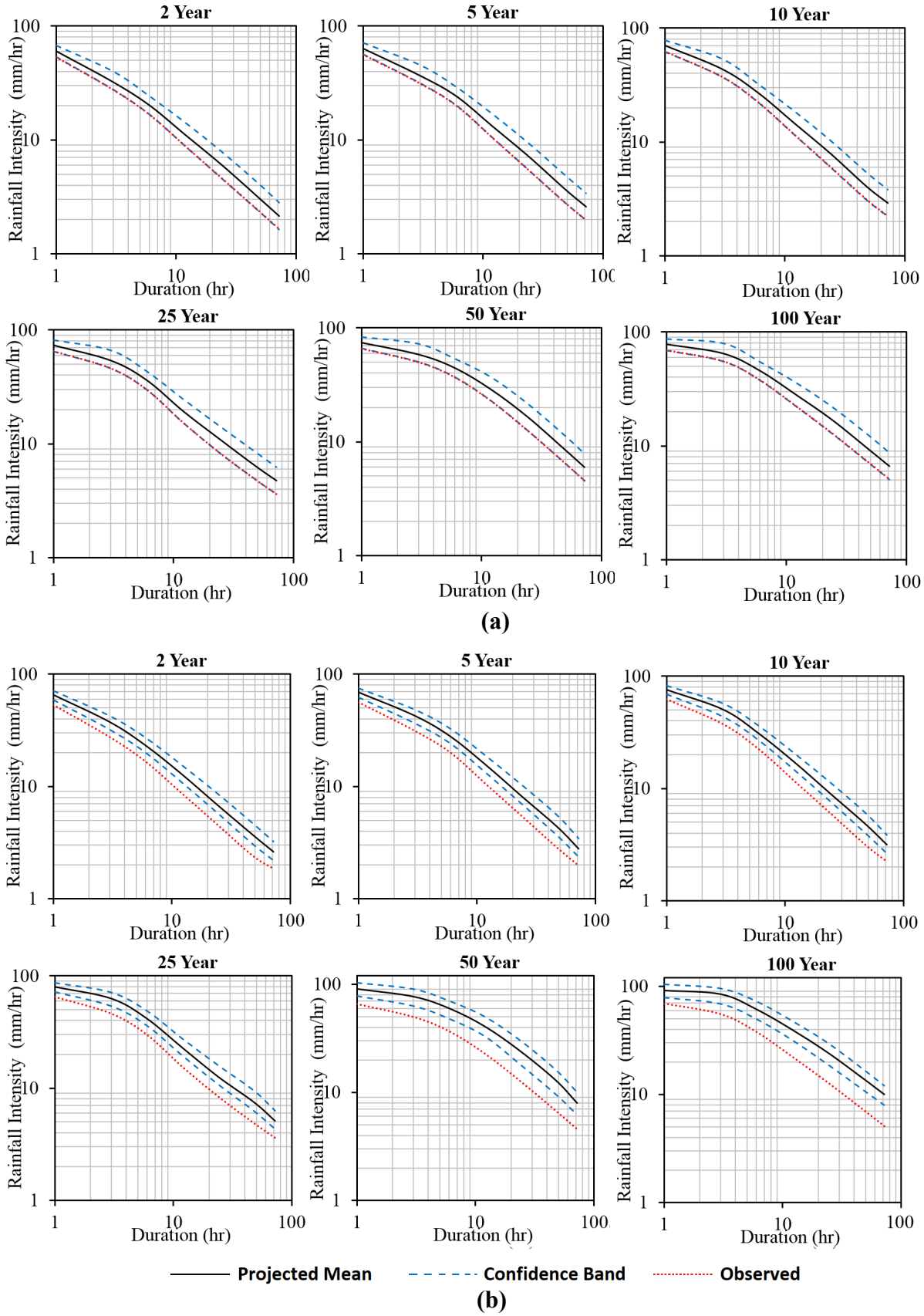

Figure 11 Projected IDF curves at a station located south of peninsular Malaysia with uncertainty for (a) RCP 2.6 and (b) RCP 8.5 during 2070-2099. The X-axis represents rainfall intensity in mm/hour, and Y-axis denotes duration in hours.

Table 3 also shows higher uncertainty in projected changes in rainfall intensities of higher return periods for all scenarios and future periods. For example, the projected changes in the 2-year RP rainfall intensity were 16.5–18.7% during 2010-2039, 10.3–21.3% during 2040-2069, and 16.7–44.1% during 2070-2099 for different RCPs. In contrast, the projected 100-year RP rainfall intensity changes were 18.7–22.2% during 2010-2039, 14.0–28.6% during 2040-2069 and 19.7–87.4 during 2070-2099. The range in the projected increase in rainfall intensity for all RPs was higher for higher RCPs. For example, the projected increase in rainfall intensity for different RPs over the whole future period (2010-2099) was in the range of 18.7– 87.4% for RCP 8.5, while the ranges were 10.3–19.7% for RCP 2.6, 7.9–23.8% for RCP 4.5, and 12.0–37.8% for RCP 6.0. The results indicate an overall increase in uncertainty in projected rainfall intensity with return period, RCPs and time in peninsular Malaysia.

Table 3 The minimum, mean and maximum changes (%) in rainfall return periods in three future periods and four RCPs

		RCP 2.6			**RCP 4.5**			**RCP 6.0**			**RCP 8.5**		
		Min	**Mean**	**Max**	**Min**	**Mean**	**Max**	**Min**	**Mean**	**Max**	**Min**	**Mean**	**Max**
2010-2039	**2**	-0.1	7.8	16.4	-2.7	7.5	17.4	5.9	14.5	22.5	5.6	13.3	24.3
	5	0.1	7.8	16.3	-2.6	7.5	17.3	5.6	14.4	22.4	5.0	12.8	23.8
	10	0.2	7.9	16.7	-2.8	7.7	17.8	5.4	14.6	23.1	4.8	12.9	24.2
	25	0.2	8.1	17.5	-3.0	8.0	18.7	5.3	15.0	24.3	4.6	13.0	25.1
	50	0.2	8.2	18.1	-3.2	8.2	19.5	5.3	15.3	25.3	4.6	13.2	25.9
	100	0.1	8.4	18.8	-3.4	8.4	20.4	5.3	15.7	26.4	4.5	13.5	26.7
2040-2069	**2**	6.1	9.8	16.4	0.1	10.1	19.1	8.7	13.1	20.1	5.7	17.6	27.1
	5	5.6	9.7	16.2	-0.4	10.0	19.0	9.0	13.0	21.0	6.0	17.5	27.2
	10	5.4	9.7	16.7	-0.5	10.1	19.6	9.1	13.2	21.8	6.0	17.8	28.5
	25	5.2	9.9	17.5	-0.7	10.4	20.7	8.8	13.5	22.9	6.0	18.5	30.6
	50	5.1	10.1	18.2	-0.9	10.6	21.7	8.7	13.8	23.8	5.9	19.1	32.5
	100	5.0	10.3	19.0	-1.0	10.9	22.7	8.7	14.1	24.7	5.9	19.7	34.5
2070-2099	**2**	-3.2	5.0	13.5	7.2	11.1	15.1	14.5	24.6	38.9	9.2	31.0	53.3
	5	-3.4	5.0	13.4	6.2	10.8	15.7	14.6	24.5	39.9	9.5	31.6	57.5
	10	-3.6	5.1	13.7	5.8	10.9	16.3	14.7	25.0	42.1	9.6	33.1	64.2
	25	-3.9	5.2	14.3	5.6	11.2	17.1	14.6	26.1	45.8	9.5	35.8	75.5
	50	-4.1	5.4	14.8	5.5	11.5	17.7	14.6	27.0	49.0	9.4	38.1	85.5
	100	-4.3	5.5	15.4	5.5	11.8	18.3	14.6	27.9	52.4	9.4	40.7	96.8

5. Discussion

Despite enhanced precipitation sensing technologies over time, satellite precipitation is still prone to high bias. It generally overestimates light precipitation and underestimates high precipitation (Nashwan et al., 2019; Ziarh et al., 2020). Underestimation of intense precipitation caused satellite precipitation to underestimate the IDF curve (Sun et al., 2019, Ombadi et al., 2018, Noor et al., 2021). The underestimation is significantly high in most cases. For example, Sun et al. (2019) showed a nearly 70% underestimation of observed IDF curves in Singapore using GSMaP. Ombadi et al. (2018) found 3 and 22% underestimation using satellite rainfall IDF curves in the US. The present study showed underestimation of observed IDF curves by 16 to 54% using GSMaP_GC. The underestimation was 8–12% for RPs higher than ten years and nearly 36–54% for RPs less than ten years. The previous studies showed successful reduction of bias in satellite IDF curves by adding or subtracting the bias for different durations and return periods (Ombadi et al., 2018; Noor et al., 2021; Venkatesh et al., 2021).

The method presented in this study assumed that the changes in rainfall distribution for different durations would be the same as the change in daily rainfall distribution. Global warming-driven rainfall changes follow a complex and spatially heterogeneous pattern. However, there is an overall assumption that shorter duration rainfall will be more intense due to climate change. However, the presently available GCMs cannot provide reliable hourly or sub-hourly rainfall estimates. Martel et al. (2021) showed that all current methods fail to estimate the future extreme rainfall. Therefore, using an available method to estimate future hourly and sub-hourly rainfall extremes adds uncertainty to projected IDF curves. Therefore, the results presented in this study should be interpreted with caution.

Previous studies showed an increase in precipitation extremes, particularly one-day maximum rainfall and rainfall intensity in peninsular Malaysia (Noor et al., 2019a; Ngai et al., 2020; Liang et al., 2021). The studies also projected a larger increase in extremes for higher emission scenarios. Therefore, the uplift of IDF curves obtained in the present study is justifiable. The present study also showed a higher increase in IDF curves for higher RCPs. However, the IDF curves were found to vary significantly over peninsular Malaysia due to variations in rainfall depth. Overall rainfall intensity was observed more on the east coast of the peninsular than on the west coast. The results agree with Khan et al. (2019). The higher uncertainty is associated with higher rainfall intensity. Therefore, the uncertainty in projected IDF was also more on the peninsula's east coast than on the west coast.

The present study showed a large bias in projected IDF curves for all RCPs. The sources of uncertainty in IDF curve projections include GCMs, projection scenarios, and the bias correction method. GCM projection uncertainty can be reduced using a GCM ensemble (Taylor et al., 2012). This study employed an ensemble of four GCMs for the projection of IDF curves. Noor et al. (2019a) evaluated the performance of all available CMIP5 GCMs in simulating the rainfall climatology of peninsular Malaysia. They suggested those four GCMs for climate change projections. The use of the ensemble of most reliable GCMs has added reliability to the IDF curves projected in this study.

The present study showed changes would be more pronounced for short duration than for high duration. This is particularly true of higher RP short-duration rainfall. For example, the intensity of the 100-year RP 1-hour duration rainfall will increase more than other durations and return periods. The results agree with Wasko and Sharma (2015) and Fadhel et al. (2017). However, it should be noted that the projected changes in rainfall depend on the considered reference period. Fadhel et al. (2017) showed that projected IDF curves significantly vary for different reference periods. This is justifiable as rainfall intensity varies on a multidecadal scale, and thus, with the reference period. This study employed 30-year (1971-2000) reference period for IDF curve projections. Generally, multidecadal climate cycles are less than 30 years. Therefore, the results obtained using 30 years as a reference period can be considered reliable. However, future studies can be conducted with different reference periods to assess uncertainty due to the reference periods.

This study employed CMIP5 GCMs to project IDF curves at ungauged locations for RCPs. Recently, CMIP6 GCMs have been released, which used the same emission scenarios used in RCPs. However, the CMIP6 GCMs also considered the global socioeconomic changes over the century and provided climate change projections for newly defined pathways known as shared socioeconomic pathways (SSPs). Therefore, mitigation, adaptation, and climate change initiatives are incorporated into SSPs based on future social and economic developments (Neill et al., 2016). The methodology used in the study can be employed in the future for the projections of IDFs for SSPs.

6. Conclusion

A methodological framework was developed in this study for generating rainfall IDF curves at ungauged locations for climate change scenarios with associated uncertainty. GSMaP_GC rainfall, observed station record and GCM rainfall simulations were used for this purpose. The

bias-corrected GSMaP_GC IDF curves could accurately replicate the observed IDF curves. Therefore, the projected IDF curves can be utilised for designing climate-resilient hydraulic structures with confidence. The short-duration higher return period rainfall intensity was projected to increase more than the long-duration lower return period. The rainfall intensity was also projected to increase more for higher emission scenarios and in the far future. Uncertainty in the projected IDF curves was found to become wide with an increase in RPs, emission scenario and time. Hence, the highest uncertainty in the projected IDF curves was found for 100-year RP for RCP 8.5 in the far future (1970-2099). Projection of IDF curves, particularly at ungauged locations, is important for long-term development planning. The procedure developed in this study can be used in any other region for reliable projection of the IDF curves for different RCPs scenarios. Besides, the uncertainty of the estimated IDF can support better decision making. In future, a study can be conducted to project IDF curves by disaggregating daily GCM rainfall to hourly rainfall and comparing the results obtained in this study. Besides, IDF can be developed for SSP scenarios and considering multiple reference periods.

References

Agilan V, Umamahesh N (2017) Nonstationary rainfall intensity-duration-frequency relationship: a comparison between annual maximum and partial duration series Water Resources Management 31:1825-1841

Ahmed K, Iqbal Z, Khan N, Rasheed B, Nawaz N, Malik I, Noor M (2019) Quantitative assessment of precipitation changes under CMIP5 RCP scenarios over the northern sub-Himalayan region of Pakistan Environment, Development and Sustainability:1-15

Alamgir M, Khan N, Shahid S, Yaseen ZM, Dewan A, Hassan Q, Rasheed B (2020) Evaluating severity–area–frequency (SAF) of seasonal droughts in Bangladesh under climate change scenarios Stochastic Environmental Research and Risk Assessment:1-18

Batisani N, Yarnal B (2010) Rainfall variability and trends in semi-arid Botswana: implications for climate change adaptation policy Applied Geography 30:483-489

Cavalcante RBL, da Silva Ferreira DB, Pontes PRM, Tedeschi RG, da Costa CPW, de Souza EB (2020) Evaluation of extreme rainfall indices from CHIRPS precipitation estimates over the Brazilian Amazonia Atmospheric Research 238:104879

Chen A, Chen D, Azorin-Molina C (2018a) Assessing reliability of precipitation data over the Mekong River Basin: A comparison of ground-based, satellite, and reanalysis datasets International Journal of Climatology 38:4314-4334

Chen J, Li C, Brissette FP, Chen H, Wang M, Essou GR (2018b) Impacts of correcting the inter-variable correlation of climate model outputs on hydrological modeling Journal of Hydrology 560:326-341

Cheng L, AghaKouchak A (2014) Nonstationary precipitation intensity-duration-frequency curves for infrastructure design in a changing climate Scientific reports 4

Elsebaie IH (2012) Developing rainfall intensity–duration–frequency relationship for two regions in Saudi Arabia Journal of King Saud University-Engineering Sciences 24:131-140

Fadhel, S., Rico-Ramirez, M. A., & Han, D. (2017). Uncertainty of intensity–duration–frequency (IDF) curves due to varied climate baseline periods. Journal of hydrology, 547, 600-612.

Feitoza Silva, D., Simonovic, S. P., Schardong, A., & Avruch Goldenfum, J. (2021). Introducing Non-Stationarity Into the Development of Intensity-Duration-Frequency Curves under a Changing Climate. Water, 13(8), 1008.

Gosset M, Alcoba M, Roca R, Cloché S, Urbani G (2018) Evaluation of TAPEER daily estimates and other GPM-era products against dense gauge networks in West Africa, analysing ground reference uncertainty Quarterly Journal of the Royal Meteorological Society 144:255-269

Hajani E, Rahman A, Ishak E (2017) Trends in extreme rainfall in the state of New South Wales, Australia Hydrological Sciences Journal 62:2160-2174

Iqbal Z, Shahid S, Ahmed K, Ismail T, Khan N, Virk ZT, Johar W (2020) Evaluation of global climate models for precipitation projection in sub-Himalaya region of Pakistan Atmospheric Research:105061

Iqbal, Z., Shahid, S., Ahmed, K., Ismail, T., Ziarh, G. F., Chung, E. S., & Wang, X. (2021). Evaluation of CMIP6 GCM rainfall in mainland Southeast Asia. Atmospheric Research, 254, 105525.

Islam MA (2018) Statistical comparison of satellite-retrieved precipitation products with rain gauge observations over Bangladesh International Journal of Remote Sensing 39:2906-2936

Jalaei, F., Guest, G., Gaur, A., & Zhang, J. (2020). Exploring the effects that a nonstationary climate and dynamic electricity grid mix has on whole building life cycle assessment: A multi-city comparison. Sustainable Cities and Society, 61, 102294.

Kalimeris A, Kolios S (2019) TRMM-based rainfall variability over the Central Mediterranean and its relationships with atmospheric and oceanic climatic modes Atmospheric Research 230:104649

Khan N, Shahid S, Chung E-S, Behlil F, Darwish MS (2020) Spatiotemporal changes in precipitation extremes in the arid province of Pakistan with removal of the influence of natural climate variability Theoretical and Applied Climatology 142:1447-1462

Khan, N., Pour, S. H., Shahid, S., Ismail, T., Ahmed, K., Chung, E. S., ... & Wang, X. (2019). Spatial distribution of secular trends in rainfall indices of Peninsular Malaysia in the presence of long-term persistence. Meteorological Applications, 26(4), 655-670.

Khazaei, M. R. (2021). A robust method to develop future rainfall IDF curves under climate change condition in two major basins of Iran. Theoretical and Applied Climatology, 144(1), 179-190.

Koutsoyiannis D, Kozonis D, Manetas A (1998) A mathematical framework for studying rainfall intensity-duration-frequency relationships Journal of Hydrology 206:118-135

Kubota, T., S. Shige, H. Hashizume, K. Aonashi, N. Takahashi, S. Seto, M. Hirose, Y. N. Takayabu, K. Nakagawa, K. Iwanami, T. Ushio, M. Kachi, and K. Okamoto, 2007: Global Precipitation Map using Satelliteborne Microwave Radiometers by the GSMaP Project : Production and Validation, IEEE Trans. Geosci. Remote Sens., 45, No. 7, 2259-2275, https://doi.org/10.1109/TGRS.2007.895337.

Langousis, A., & Veneziano, D. (2007). Intensity-duration-frequency curves from scaling representations of rainfall. Water Resources Research, 43(2).

Leander R, Buishand TA (2007) Resampling of regional climate model output for the simulation of extreme river flows Journal of Hydrology 332:487-496

Liang, J., Tan, M. L., Hawcroft, M., Catto, J. L., Hodges, K. I., & Haywood, J. M. (2021). Monsoonal precipitation over Peninsular Malaysia in the CMIP6 HighResMIP experiments: the role of model resolution. Climate Dynamics, 1-23.

Liu J, Shangguan D, Liu S, Ding Y, Wang S, Wang X (2019) Evaluation and comparison of CHIRPS and MSWEP daily-precipitation products in the Qinghai-Tibet Plateau during the period of 1981–2015 Atmospheric Research 230:104634

Mahmoud MT, Hamouda MA, Mohamed MM (2019) Spatiotemporal evaluation of the GPM satellite precipitation products over the United Arab Emirates Atmospheric research 219:200-212

Martel, J. L., Brissette, F. P., Lucas-Picher, P., Troin, M., & Arsenault, R. (2021). Climate Change and Rainfall Intensity–Duration–Frequency Curves: Overview of Science and Guidelines for Adaptation. *Journal of Hydrologic Engineering*, *26*(10), 03121001.

Mayowa OO, Pour SH, Shahid S, Mohsenipour M, Harun SB, Heryansyah A, Ismail T (2015) Trends in rainfall and rainfall-related extremes in the east coast of peninsular Malaysia Journal of Earth System Science 124:1609-1622

Nashwan M, Shahid S, Chung E-S, Ahmed K, Song Y (2018) Development of Climate-Based Index for Hydrologic Hazard Susceptibility. Sustainability 10:2182

Nashwan MS, Shahid S (2020) A novel framework for selecting general circulation models based on the spatial patterns of climate International Journal of Climatology

Ngai, S. T., Sasaki, H., Murata, A., Nosaka, M., Chung, J. X., Juneng, L., ... & Tangang, F. (2020). Extreme rainfall projections for malaysia at the end of 21st century using the high resolution non-hydrostatic regional climate model (NHRCM). SOLA.

Noor M, bin Ismail T, Shahid S, Ahmed K, Chung E-S, Nawaz N (2019a) Selection of CMIP5 multi-model ensemble for the projection of spatial and temporal variability of rainfall in peninsular Malaysia Theoretical and Applied Climatology 138:999-1012

Noor M, Ismail T, Chung E-S, Shahid S, Sung JH (2018) Uncertainty in rainfall intensity duration frequency curves of peninsular Malaysia under changing climate scenarios Water 10:1750

Noor M, Ismail T, Shahid S, Asaduzzaman M, Dewan A (2021) Evaluating intensity-duration-frequency (IDF) curves of satellite-based precipitation datasets in Peninsular Malaysia Atmospheric Research, 248, 105203

Noor M, Ismail T, Shahid S, Nashwan MS, Ullah S (2019b) Development of multi-model ensemble for projection of extreme rainfall events in Peninsular Malaysia Hydrology Research 50:1772-1788

Oberascher, M., Rauch, W., & Sitzenfrei, R. (2022). Towards a smart water city: A comprehensive review of applications, data requirements, and communication technologies for integrated management. Sustainable Cities and Society, 76, 103442.

Okamoto Ki, Ushio T, Iguchi T, Takahashi N, Iwanami K (2005) The Global Satellite Mapping of Precipitation (GSMaP) project vol 5. doi:10.1109/IGARSS.2005.1526575

Ombadi, M., Nguyen, P., Sorooshian, S., & Hsu, K. L. (2018). Developing intensity-duration-frequency (IDF) curves from satellite-based precipitation: Methodology and evaluation. Water Resources Research, 54(10), 7752-7766.

Ou T, Chen D, Linderholm HW, Jeong J-H (2013) Evaluation of global climate models in simulating extreme precipitation in China Tellus A: Dynamic Meteorology and Oceanography 65:19799

Ouarda TB, Yousef LA, Charron C (2019) Non-stationary intensity-duration-frequency curves integrating information concerning teleconnections and climate change International Journal of Climatology 39:2306-2323

Peck, A., Prodanovic, P., Slobodan P., Simonovic, P. (2012). Rainfall Intensity Duration Frequency Curves Under Climate Change: City of London, Ontario, Canada. Canadian Water Resources Journal, 37(3)

Peng J et al. (2020) A pan-African high-resolution drought index dataset Earth System Science Data 12:753-769

Pour SH, Abd Wahab AK, Shahid S, Dewan A (2020) Low Impact Development Techniques to Mitigate the Impacts of Climate-Change-Induced Urban Floods: Current Trends, Issues and Challenges Sustainable Cities and Society:102373

Pour SH, Harun SB, Shahid S (2014) Genetic programming for the downscaling of extreme rainfall events on the east coast of peninsular Malaysia Atmosphere 5:914-936

Pour, S. H., Abd Wahab, A. K., Shahid, S., & Ismail, Z. B. (2020). Changes in reference evapotranspiration and its driving factors in peninsular Malaysia. Atmospheric Research, 246, 105096.

Ragno, E., AghaKouchak, A., Love, C. A., Cheng, L., Vahedifard, F., & Lima, C. H. R. (2018). Quantifying Changes in Future Intensity-Duration-Frequency Curves Using Multimodel Ensemble Simulations. Water Resources Research, 54(3), 1751–1764. https://doi.org/10.1002/2017WR021975

Reddy MV, Mitra AK, Momin IM, Mitra AK, Pai D (2019) Evaluation and inter-comparison of high-resolution multi-satellite rainfall products over India for the southwest monsoon period International journal of remote sensing 40:4577-4603

Rodríguez R, Navarro X, Casas MC, Ribalaygua J, Russo B, Pouget L, Redaño A (2014) Influence of climate change on IDF curves for the metropolitan area of Barcelona (Spain) International journal of climatology 34:643-654

Salman, S. A., Nashwan, M. S., Ismail, T., & Shahid, S. (2020). Selection of CMIP5 general circulation model outputs of precipitation for peninsular Malaysia. Hydrology Research, 51(4), 781-798.

Samadi S, Sagareswar G, Tajiki M (2010) Comparison of general circulation models: methodology for selecting the best GCM in Kermanshah Synoptic Station, Iran International Journal of Global Warming 2:347-365

Shahid S (2011) Trends in extreme rainfall events of Bangladesh Theoretical and applied climatology 104:489-499

Sharifi E, Eitzinger J, Dorigo W (2019) Performance of the State-Of-The-Art Gridded Precipitation Products over Mountainous Terrain: A Regional Study over Austria Remote Sensing 11:2018

Shawky M, Moussa A, Hassan QK, El-Sheimy N (2019) Performance Assessment of Sub-Daily and Daily Precipitation Estimates Derived from GPM and GSMaP Products over an Arid Environment Remote Sensing 11:2840

Suhaila J, Jemain AA (2009) A comparison of the rainfall patterns between stations on the East and the West coasts of Peninsular Malaysia using the smoothing model of rainfall amounts Meteorological Applications 16:391-401

Taylor, K. E., Stouffer, R. J., & Meehl, G. A. (2012). An overview of CMIP5 and the experiment design. Bulletin of the American meteorological Society, 93(4), 485-498.

Tousi, E. G., O'Brien, W., Doulabian, S., & Toosi, A. S. (2021). Climate changes impact on stormwater infrastructure design in Tucson Arizona. Sustainable Cities and Society, 72, 103014.

Trenberth KE (2011) Changes in precipitation with climate change Climate Research 47:123-138

Ushio T et al. (2009) A Kalman filter approach to the Global Satellite Mapping of Precipitation (GSMaP) from combined passive microwave and infrared radiometric data Journal of the Meteorological Society of Japan Ser II 87:137-151

Venkatesh, K., Maheswaran, R., & Devacharan, J. (2021). Framework for developing IDF curves using satellite precipitation: a case study using GPM-IMERG V6 data. Earth Science Informatics, 1-17.

Wasko, C., & Sharma, A. (2015). Steeper temporal distribution of rain intensity at higher temperatures within Australian storms. *Nature Geoscience*, *8*(7), 527-529.

Yan H, Sun N, Wigmosta M, Skaggs R, Hou Z, Leung LR (2019) Next-generation intensity–duration–frequency curves to reduce errors in peak flood design Journal of Hydrologic Engineering 24:04019020

Yao J, Chen Y, Yu X, Zhao Y, Guan X, Yang L (2020) Evaluation of multiple gridded precipitation datasets for the arid region of northwestern China Atmospheric Research 236:104818

Yatagai A, Arakawa O, Kamiguchi K, Kawamoto H, Nodzu MI, Hamada A (2009) A 44-year daily gridded precipitation dataset for Asia based on a dense network of rain gauges Sola 5:137-140

Yilmaz A, Perera B (2014) Extreme rainfall nonstationarity investigation and intensity–frequency–duration relationship Journal of Hydrologic Engineering 19:1160-1172

Young, A. F., & Papini, J. A. J. (2020). How can scenarios on flood disaster risk support urban response? A case study in Campinas Metropolitan Area (São Paulo, Brazil). Sustainable Cities and Society, 61, 102253.

Ziarh, G. F., Shahid, S., Ismail, T. B., Asaduzzaman, M., & Dewan, A. (2021). Correcting bias of satellite rainfall data using physical empirical model. *Atmospheric Research*, *251*, 105430.

Supplementary Materials

Table S1 Description of the 80 rainfall observation stations used in the present study

No.	Station ID	Longitude	Latitude	Elevation	Annual Rainfall
1	Johor 1437116	103.7528	1.4708	26	2535.2
*2	Johor 1541139	104.1847	1.5264	38	1813.9
3	Johor 1737001	103.7194	1.7639	49	1928.6
*4	Johor 2025001	102.5778	2.0514	7	1699.7
5	Johor 2237164	103.7361	2.2569	35	2226.6
*6	Johor 2534160	103.4194	2.5389	30	3279.8
7	Johor 2636170	103.6208	2.65	8	2463.7
*8	Kedah 5806066	100.6319	5.8139	38	2340.2
9	Kedah 5808001	100.8944	5.8806	160	2252.5
10	Kedah 6103047	100.3917	6.1056	6	2013.1
11	Kedah 6108001	100.8472	6.1056	128	2181.3
12	Kedah 6206035	100.6125	6.2542	32	1924.8
13	Kedah 6207032	100.7722	6.2403	124	1788.1
14	Kedah 6306031	100.6903	6.3431	41	1594.6
15	Kelanatan 4819027	101.9694	4.8792	127	2227.9
16	Kelanatan 4923001	102.3528	4.9375	88	2433.8
17	Kelanatan 5320038	102.0153	5.3778	47	2281.6
*18	Kelanatan 5322044	102.275	5.3083	52	2290.7
19	Kelanatan 5522047	102.2028	5.5319	34	2329.3
20	Kelanatan 5718033	101.8389	5.7014	88	2302
*21	Kelanatan 6019004	101.9792	6.0236	11	3113.3
22	Melaka 2224038	102.4917	2.2889	20	1680.2
23	Melaka 2321006	102.1931	2.3639	48	1481.5
24	N.Sembilan 2719001	101.9556	2.7375	69	2245.4
25	N.Sembilan 2725083	102.5125	2.7194	77	1549.7
*26	N.Sembilan 3020016	102.0736	3.0931	163	1818.9
27	Pahang 2828173	102.8556	2.85	42	1341.6
28	Pahang 2924096	102.4189	2.9375	71	1194.3
29	Pahang 3121143	102.1972	3.175	84	1502.3
*30	Pahang 3129177	102.9764	3.1681	43	1681.2
31	Pahang 3134165	103.4417	3.1375	10	1942.4
32	Pahang 3231163	103.1889	3.2875	19	2353
33	Pahang 3330109	103.0264	3.3903	27	1960.5
34	Pahang 3424081	102.42	3.43	40	1149.1
35	Pahang 3519125	101.9153	3.5125	115	1942.3
*36	Pahang 3533102	103.3569	3.5611	5	2509.6
37	Pahang 3628001	102.8556	3.6333	71	1598
*38	Pahang 3924072	102.4333	3.9042	52	1759.5

No.	Station ID	Longitude	Latitude	Elevation	Annual Rainfall
39	Pahang 4023001	102.325	4.0319	65	1714.4
40	Pahang 4219001	101.9403	4.2333	99	1797.4
41	Pahang 4324001	102.4028	4.3861	91	1836.3
42	Pahang 4513033	101.3833	4.5167	1832	2066.7
43	Perak 3615003	101.5236	3.6833	45	2583.9
44	Perak 4010001	101.0361	4.0167	6	2215.1
45	Perak 4012143	101.3	4.0486	44	2263.6
*46	Perak 4207048	100.7	4.2181	7	1399.4
47	Perak 4209093	100.9	4.2556	16	1973.3
48	Perak 4311001	101.1556	4.3056	208	3154.9
49	Perak 4409091	100.9014	4.4611	26	1712.1
50	Perak 4511111	101.125	4.5889	50	2238.9
51	Perak 4611001	101.1694	4.6806	98	1959.7
52	Perak 4708084	100.8944	4.775	98	1668.3
53	Perak 4807016	100.7931	4.8625	864	3220.6
54	Perak 4811075	101.175	4.8931	111	1643.3
55	Perak 4908018	100.8042	4.9792	43	2050.2
56	Perak 5005003	100.5458	5.0139	3	1485.9
57	Perak 5207001	100.7014	5.2167	22	2036.6
*58	Perak 5210069	101.0583	5.2986	115	1597.6
59	Perak 5411066	101.1542	5.4167	132	1721.2
60	Perak 5610063	101.0806	5.6042	198	1658
61	Perak 5710061	101	5.7083	334	1754.4
62	Perlis 6401002	100.1875	6.4458	7	1681.6
*63	Perlis 6603002	100.3097	6.6569	69	1507.3
64	Pinang 5504035	100.4306	5.5347	5	2083.7
65	Selangor 2913001	101.3931	2.9306	8	1624.5
66	Selangor 3118102	101.8722	3.1736	104	2358.1
*67	Selangor 3314001	101.4122	3.3689	9	1669.4
68	Selangor 3411017	101.1733	3.4236	4	1533.5
69	Selangor 3710006	101.0831	3.7286	6	1593.1
70	Terengganu 4234109	103.4222	4.2319	8	2776.7
*71	Terengganu 4734079	103.4194	4.7625	10	2683.9
*72	Terengganu 4929001	102.9667	4.9528	38	4065.7
73	Terengganu 4930038	103.0611	4.9389	32	3740.7
74	Terengganu 5029034	102.9417	5.0667	25	3513.4
75	Terengganu 5328044	102.8861	5.3556	29	3755.3
76	Terengganu 5331048	103.1333	5.3181	3	2548.9
77	Terengganu 5426001	102.675	5.4764	40	4409.6
78	WP 3116003	101.6847	3.1514	63	2818
79	WP 3216001	101.6861	3.2722	137	2444.8
80	WP 3317004	101.7708	3.3681	1004	2551.7

*Stations used for validation

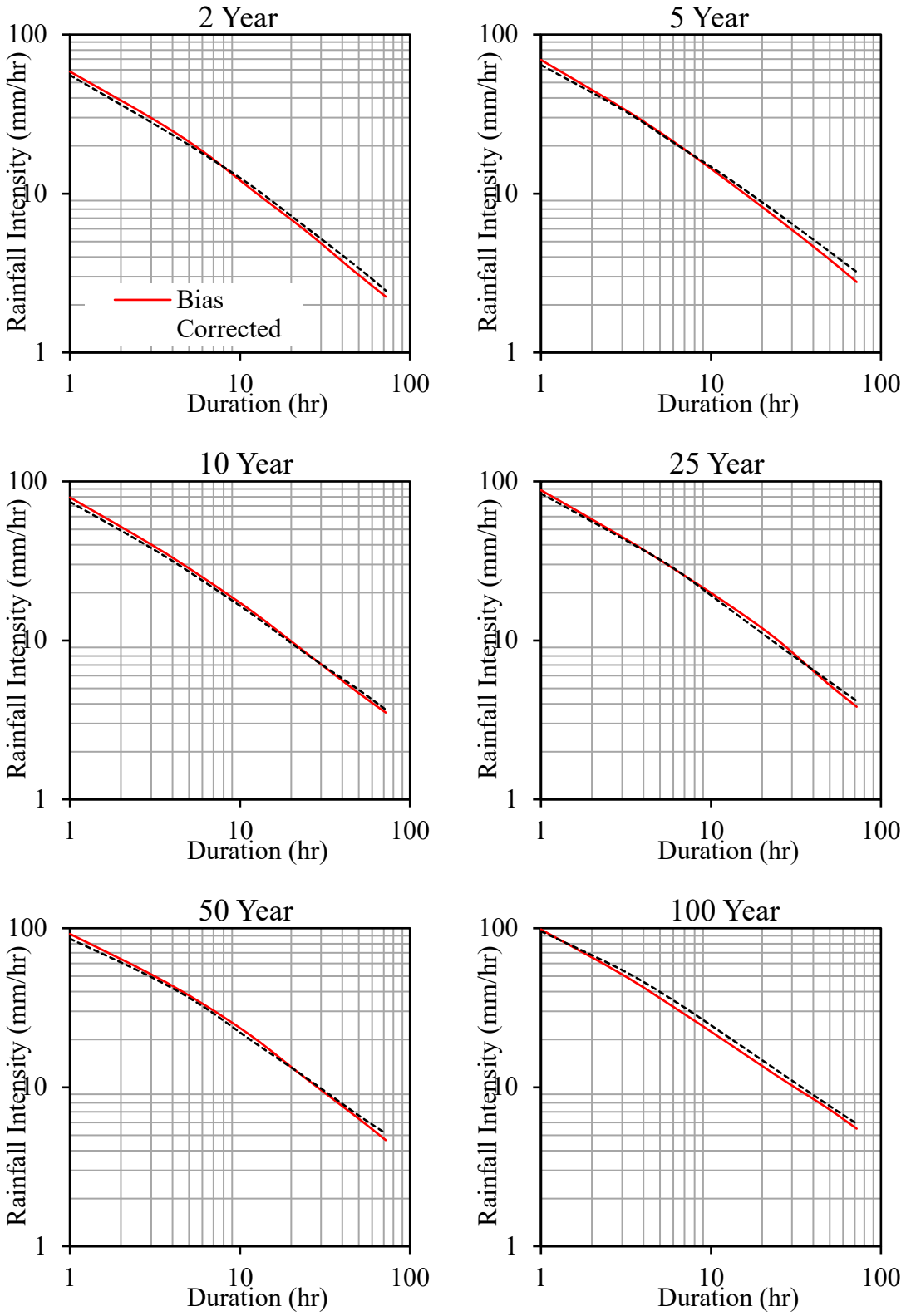

Figure S-1 In-situ and bias-corrected GSMaP_GC IDF curves for different return periods at a station located in central peninsular Malaysia (PAHANG 3129177)